

A Scalable Platform for Fabricating Biodegradable Microparticles with Pulsatile Drug Release

Tyler P. Graf, Sherry Yue Qiu, Dhruv Varshney, Mei-Li Laracuente, Erin M. Euliano, Pujita Munnangi, Brett H. Pogostin, Tsvetelina Baryakova, Arnav Garyali, and Kevin J. McHugh*

Pulsatile drug delivery systems have the potential to improve patient adherence and therapeutic efficacy by providing a sequence of doses in a single injection. Herein, a novel platform, termed Particles Uniformly Liquified and Sealed to Encapsulate Drugs (PULSED) is developed, which enables the high-throughput fabrication of microparticles exhibiting pulsatile release. In PULSED, biodegradable polymeric microstructures with an open cavity are formed using high-resolution 3D printing and soft lithography, filled with drug, and sealed using a contactless heating step in which the polymer flows over the orifice to form a complete shell around a drug-loaded core. Poly(lactic-co-glycolic acid) particles with this structure can rapidly release encapsulated material after delays of 10 ± 1 , 15 ± 1 , 17 ± 2 , or 36 ± 1 days *in vivo*, depending on polymer molecular weight and end group. The system is even compatible with biologics, releasing over 90% of bevacizumab in its bioactive form after a two-week delay *in vitro*. The PULSED system is highly versatile, offering compatibility with crystalline and amorphous polymers, easily injectable particle sizes, and compatibility with several newly developed drug loading methods. Together, these results suggest that PULSED is a promising platform for creating long-acting drug formulations that improve patient outcomes due to its simplicity, low cost, and scalability.

1. Introduction

Pharmaceuticals have revolutionized the way diseases are treated. Today, more than 50% of the world's population

takes at least one medication every day, contributing to a global market estimated at \$1.27 trillion.^[1,2] Despite the success of therapeutics and prophylactics in prolonging life and improving quality of life, these benefits are limited by poor patient adherence, which can be as low as 50% in patients with chronic conditions.^[3–5] This lack of patient adherence contributes to negative outcomes, including death, and results in an additional \$289 billion in healthcare costs each year in the United States alone.^[6–8] Reducing drug dosing frequency has been identified as one of the most effective means to increase patient adherence.^[9,10] However, many diseases including diabetes, cancer, human immunodeficiency virus infection, depression, and autoimmune disorders, are typically treated with frequent, repeated, and long-term administration of therapeutics, often as frequently as multiple times a day, to maintain drug levels that are both safe and effective. Controlled drug delivery systems represent a promising solution to mitigate

compliance issues. By releasing drugs over an extended period of time, these systems can be administered less frequently, thereby improving adherence and patient outcomes. For example, the FDA-approved Lupron Depot, composed of drug-loaded biodegradable microspheres, has been shown to improve patient adherence and convenience by reducing administration frequency from a once-daily injection to one injection every one to six months.^[11,12]

Oral delivery systems are convenient, but their rapid passage through the gastrointestinal tract limits their duration of action, often requiring frequent re-dosing that can lead to lower levels of patient adherence compared to less frequent parenteral injection(s).^[13] Unfortunately, most injectable controlled-release systems generate an initial burst release followed by first-order release kinetics in which drug is released at a perpetually lower rate over time.^[14,15] Although these devices extend the duration of drug activity, their front-loaded and slowing rate of release limits their ability to maintain therapeutic efficacy over a long period of time, especially when the biological half-life of the drug is short or the therapeutic window is small. Increasing initial drug loading can extend the duration of release in these

T. P. Graf, S. Y. Qiu, D. Varshney, M.-L. Laracuente, E. M. Euliano, P. Munnangi, B. H. Pogostin, T. Baryakova, A. Garyali, K. J. McHugh
Department of Bioengineering

Rice University
Houston, TX 77005, USA
E-mail: kevin.mchugh@rice.edu

M.-L. Laracuente
Medical Scientist Training Program
Baylor College of Medicine
Houston, TX 77030, USA
K. J. McHugh
Department of Chemistry
Rice University
Houston, TX 77005, USA

The ORCID identification number(s) for the author(s) of this article can be found under <https://doi.org/10.1002/adma.202300228>.

DOI: 10.1002/adma.202300228

devices but may also cause toxic levels of the drug to be released during the early rapid-release phase.

Implantable devices have overcome this challenge through the use of more sophisticated mechanisms (e.g., pumps),^[16] but require a medical procedure for implantation and are not fully biodegradable, typically necessitating a follow-up procedure for removal.^[17] Biodegradable microparticle systems that exhibit delayed, pulsatile drug release are a promising alternative to implantable systems and microparticles with first-order release kinetics. By administering a combination of distinct particle populations that each release a therapeutic as a bolus dose on a different day, a single injection can be used to mimic the pharmacokinetics of traditional drug dosing regimens known to be safe and effective without the need for frequent re-administration. Further, because they do not exhibit the initial “time-zero” burst followed by first-order release kinetics that most FDA-approved injectable systems demonstrate, their duration of efficacy is not inherently limited.^[18,19] An injectable system reduces the burden of administration compared to implantable systems and greatly expands the number of potential use cases.

Broadly speaking, pulsatile drug delivery systems are either triggered by a stimulus^[20–23] or are passively degraded in the body.^[24,25] Because the former requires patient action, which is a key challenge we are trying to overcome, we elected to create a system that degrades passively. One of the first passive pulsatile release systems developed consisted of a polymeric microchip using multiple materials to achieve distinct pulsatile release at time points ranging from 0 to 40 days.^[26] Although this device achieved unprecedented release kinetics for a passively degrading system, its large size (12 mm diameter) and non-degradable components tempered clinical excitement. Since then, many groups have sought to overcome these limitations by recreating the release kinetics using injectable particles that are fully biodegradable. However, these systems have suffered from substantial drug release during the initial “delay” phase, exhibit broad periods of drug release that can span weeks, and/or are costly to scale, limiting their potential for commercialization and clinical use.^[27–30]

Recently, a multi-layer polymer sintering process was used to generate fully biodegradable particles exhibiting delayed pulsatile release.^[31] Termed the StampEd Assembly of polymer Layers (SEAL), this fabrication process represented a significant step forward in achieving pulsatile release kinetics in an injectable, fully biodegradable delivery system. Several aspects of this process make it difficult to increase throughput, manage production costs, and efficiently produce small particles suitable for injection through small-diameter needles. In particular, the multi-component alignment step of the SEAL process requires highly specialized equipment and is complicated by misalignment due to non-uniform polydimethylsiloxane (PDMS) deformation.^[32–35] To overcome these limitations, we developed a streamlined alternative that enables the use of equipment commonly found in research labs to create drug-loaded microparticles that exhibit both delayed and tunable pulsatile release kinetics. This facile process, termed Particles Uniformly Liquified and Sealed to Encapsulate Drug (PULSED), has several key advantages that make it technically and commercially superior to its predecessors. First, it is imminently scalable, enabling low-cost, high-throughput production. Second, it can create

microparticles small enough to readily flow through even the smallest commonly used needles. Third, it is compatible with both amorphous and crystalline polymers. Last, its one-component assembly method leads to higher production consistency and therefore fewer quality control concerns.

2. Results and Discussion

To create particles with the requisite core-shell structure, we first fabricated hollow cylinders with a solid base using multi-photon 3D printing to enable rapid prototyping for various particle geometries (Figure S1a, Supporting Information). An inverse mold was then generated via soft lithography using PDMS, as seen in Figure S1b,c, Supporting Information. To minimize potential damage to the original 3D-printed master mold, we then used the PDMS inverse molds to cast mechanically robust arrays composed of a photocurable polymer (Figure S1d–f, Supporting Information). Iterating this step enabled the production of multiple master mold replicates, facilitating quick replication of subsequent inverse PDMS molds (Figure S1g–i, Supporting Information). Poly(lactic-co-glycolic acid) (PLGA), a biocompatible polymer used in numerous FDA-approved drug delivery formulations, was then used to make films. Four PLGA polymers were explored as a means to alter the degradation rate and thus release timing. All of these materials had a copolymer ratio of 50:50 lactic acid:glycolic acid but varied in weight-average molecular weight (M_w) and end group (Table S1, Supporting Information). These materials have a M_w of 13 kDa with a carboxylic acid end group (PLGA_{13COOH}), a M_w of 42 kDa with a carboxylic acid end group (PLGA_{42COOH}), a M_w of 34 kDa with an ester end group (PLGA_{34COOR}), or a M_w of 87 kDa with an ester end group (PLGA_{87COOR}). PLGA films were then compressed into PDMS molds while heated above their glass transition temperature under vacuum to generate arrays of open-faced particles (Figure 1a,b). Despite the number of replication steps, PLGA microparticle structure remained highly consistent, reproducing even small topographical features throughout the process. The particles displayed minimal decreases in diameter, wall thickness, and height of only $1.8 \pm 0.3\%$, $3.2 \pm 1.5\%$, and $2.7 \pm 0.8\%$, respectively when compared to the original array (Figure S2, Supporting Information).

Open-faced PLGA particles were next filled with a model drug solution using a piezoelectric dispensing device. In this step, a drug solution is ejected into the particle core and the volatile solvent, typically water, rapidly evaporates, leaving the previously dissolved drug behind in the particle core as a solid (Figure 1c,d). Filled open-faced particles were inverted and placed over a level heated surface to bring PLGA at the top of the cylinder above its glass transition temperature. In this state, the polymer begins to flow and close the open face of the model drug-filled cylinders—likely as a product of surface tension and gravity—to form a contiguous polymer shell around the internal drug depot (Figure 1e,f). Following the sealing, the particles were then removed from heat and cooled at room temperature to prevent further deformation.

To visualize and optimize this process, we heated particles composed of PLGA_{13COOH} for 0, 6, 12, 18, 24, 30, and 36 s and then imaged the resulting microstructures using a

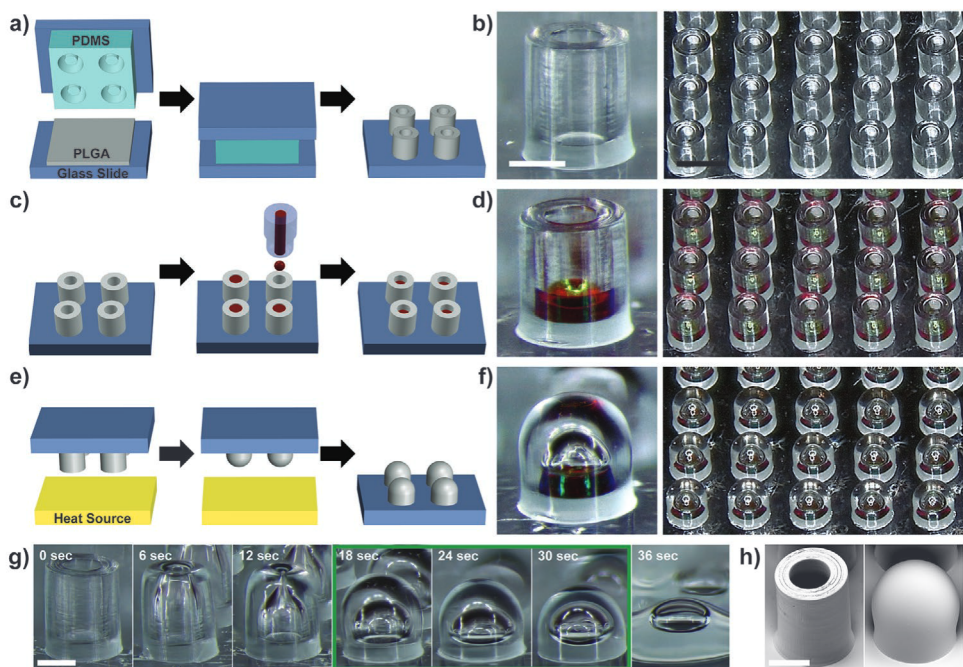


Figure 1. PULSED microparticle fabrication and sealing. a) Polymer films are compressed into PDMS molds, placed under vacuum, and heated above the polymer's melting point or glass transition temperature to create open-faced microparticles. b) Stereoscope images of open-faced cylindrical microparticles. c) Arrays of microparticles are filled via the dropwise addition of a drug solution into the core using a piezoelectric dispensing system. The solvent (e.g., water) then evaporates, leaving behind the drug in solid form. d) Representative stereoscope images of microparticles filled with 3 µg of fluorescein sodium salt. e) Filled microstructures are inverted and placed over a heat source, causing the polymer to flow and seal the open face of the microparticle. f) Stereoscope images of sealed microparticles. g) Stereoscope images of particles held over the heat source for various durations. Note: The green box indicates the range of acceptable microparticle sealing times for PLGA₁₃COOH. h) SEM image of particles before and after sealing for 18 s. Scale bars: black = 500 µm, white = 200 µm. All images show microstructures composed of PLGA₁₃COOH.

stereomicroscope after particles had cooled. As seen in Figure 1g and Video S1, Supporting Information, the open face of the cylindrical particles slowly began to close before fully sealing between 12 and 18 s. The desired structure is maintained through 30 s but is lost by 36 s. Therefore, a sealing time of 18 s was used for PLGA₁₃COOH in all subsequent experiments. Scanning electron microscopy (SEM) images of an unsealed PLGA₁₃COOH particle and a PLGA₁₃COOH particle sealed for 18 s are shown in Figure 1h. A similar process was used to determine the appropriate sealing time for PLGA₄₂COOH, PLGA₃₄COOR, and PLGA₈₇COOR, resulting in optimal sealing times of 38, 42, and 60 s, respectively.

Next, to show that microparticles produced using the PULSED method exhibit pulsatile release, microparticles made with PLGA were filled with 10 kDa dextran labeled with Alexa Fluor 647 as a model of a macromolecule drug. Release kinetics were determined by incubating microparticles in phosphate-buffered saline (PBS) at 37 °C under agitation to simulate in vivo conditions and sampling the supernatant daily close to the expected release. All PLGA particles showed pulsatile drug release in vitro after a temporal delay that was dependent on polymer molecular weight and end-group. PLGA₁₃COOH, PLGA₄₂COOH, PLGA₃₄COOR, and PLGA₈₇COOR microparticles released a majority of their cargo by day 8 ± 0, 14 ± 1, 18 ± 1, and 31 ± 1 in vitro, respectively (Figure 2a). In addition, each particle's release was rapid, with 75% of the model drug releasing over a period of 2 ± 0 (PLGA₁₃COOH), 2 ± 1 (PLGA₄₂COOH),

3 ± 1 (PLGA₃₄COOR), and 1 ± 1 (PLGA₈₇COOR) days. Furthermore, the individual particles had highly uniform release characteristics, highlighting the consistency of the PULSED fabrication process (Figure S3, Supporting Information). Increasing molecular weight and/or the addition of an ester cap produced longer delays, which is in agreement with previously published observations.^[36,37] In addition, alteration of the ratio of lactic acid to glycolic acid monomers, and degree of crystallinity are other mechanisms that have been reported to affect PLGA release profiles, and could be further explored to tune release kinetics.^[38]

To demonstrate the platform's ability to deliver small molecules—a key category of drug that composes approximately 90% of pharmaceutical drugs^[39]—in a pulsatile manner, we evaluated the release of fluorescein sodium salt (molecular weight = 376.27 Da) from PLGA₁₃COOH PULSED microparticles. Release kinetics of the small molecule was similar to that of the dextran-Alexa Fluor 647 macromolecule, releasing on day 8 ± 1 and 8 ± 0, respectively. Of note however, the duration required to release 75% of the small molecule was slightly longer at 3 ± 1 days compared to the macromolecule release at 2 ± 0 days (Figure S4, Supporting Information).

In order to determine in vivo release kinetics, we employed an In Vivo Imaging System (IVIS, PerkinElmer, Hopkinton, MA) to track the release of a fluorescent payload from PULSED microparticles. We validated a previously existing in vivo quantification method,^[31,36,40] by monitoring the release of

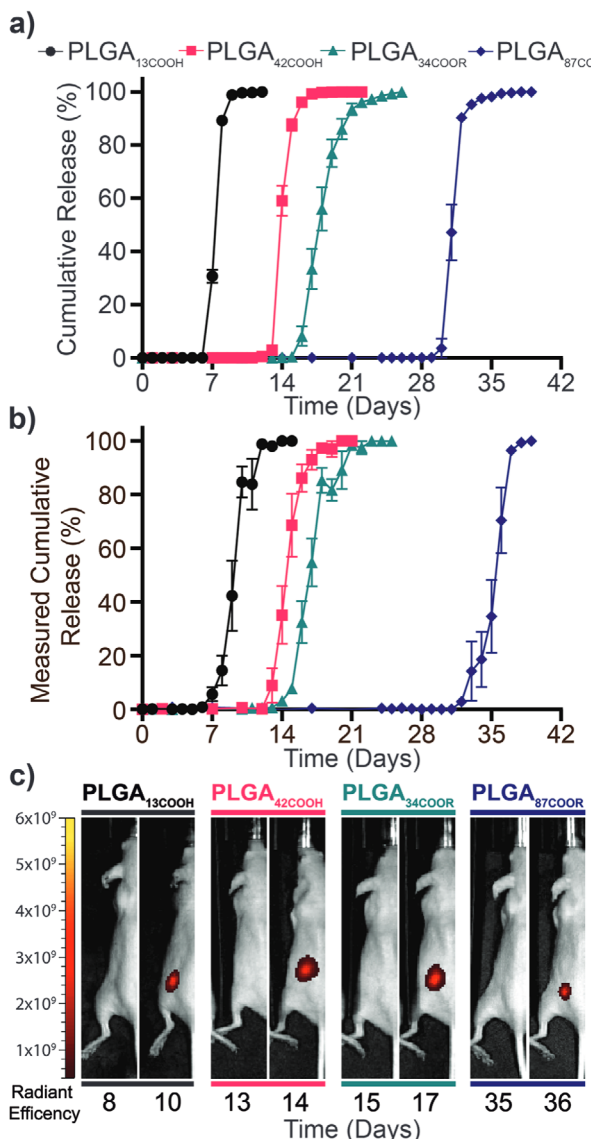


Figure 2. In vitro and in vivo release of a model drug from PULSED microparticles. a) Normalized in vitro cumulative release of Alexa Fluor 647-labeled 10 kDa dextran from microparticles composed of four different types of PLGA incubated in PBS at 37 °C ($n=11-12$). b) Normalized in vivo cumulative release of Alexa Fluor 647-labeled 10 kDa dextran from four sets of PLGA particles injected subcutaneously into the rear flank of SKH1-Elite mice ($n=6-9$). c) Representative photographs with fluorescence overlay showing Alexa Fluor 647-labeled 10 kDa dextran release from four types of PLGA particles in mice. Radiant efficiency is shown in units of $(\text{p s}^{-1} \text{cm}^{-1} \text{sr}^{-1}) (\mu\text{W cm}^{-2})^{-1}$. All error bars indicate standard error of the mean.

Alexa Fluor 647-labeled 10 kDa dextran from PLGA particles incubated in a 96-well plate. As previously demonstrated, fluorescent signal was not detected until the release of the Alexa Fluor 647-labeled 10 kDa dextran, likely due to the high concentration of the dye self-quenching prior to release. Upon release, the fluorescent signal increases several orders of magnitude as the dye dissipates. As expected, the quantified release from this validation experiment (Figure S5, Supporting Information) closely matched the release kinetics presented in Figure 2a.

After validating the quantification method, SKH1-Elite mice were subcutaneously injected with a single PULSED particle filled with Alexa Fluor 647-labeled 10 kDa dextran. In vivo release of the fluorescent macromolecule was measured non-invasively using an IVIS. Release kinetics remained tunable in vivo based on polymer properties with particles releasing on days 10 ± 1 , 15 ± 1 , 17 ± 1 , and 36 ± 1 for PLGA_{13COOH}, PLGA_{42COOH}, PLGA_{34COOR}, and PLGA_{87COOR}, respectively (Figure 2b). Additionally, the release from individual particles remained highly pulsatile, with 75% of each particle's measured fluorescence signal releasing over periods of 2 ± 1 (PLGA_{13COOH}), 2 ± 1 (PLGA_{42COOH}), 3 ± 1 (PLGA_{34COOR}), and 2 ± 1 (PLGA_{87COOR}) days. Figure 2c shows representative images of mice that illustrate the rapid increase in fluorescence over 24 to 48 h.

After confirming that single-particle injections exhibit rapid pulsatile release in vivo, we sought to investigate the potential impact that injecting multiple particles would have on in vivo release, since many applications will require a release from more than one particle and/or at more than one time point. To investigate the effects of other particles being present, five particles from each of the four PLGA formulations (20 particles total) were injected into mice. Each group contained PULSED microparticles of only one PLGA type, while the remaining 15 PLGA PULSED particles composed of the other three PLGA types were empty. The number of particles injected did not have a significant effect on release kinetics according to a two-way ANOVA (Figure S6, Supporting Information), suggesting that PULSED particle release is largely unaffected by the presence of other particle populations.

So far, these in vitro experiments have assumed typical conditions in which the pH and temperature are 7.4 and 37 °C, respectively. However, some disease states can alter the particle microenvironment. Cancer for example maintains intertumoral pH that can reach as low as 6,^[41,42] while fevers can increase body temperature. We sought to explore the effect of these parameters on release kinetics. When incubated in solutions within the intertumoral pH range, the release kinetics from PLGA_{42COOH} microparticles remained statistically similar with release occurring on days 13 ± 1 (pH 7.4), 14 ± 1 (pH 6.5), and 14 ± 1 (pH 6). It was not until particles were incubated at a pH of 4 that an accelerated release of 11 ± 1 days was observed, likely due to acid-catalyzed hydrolysis of PLGA (Figure S7a, Supporting Information). When particles were incubated at different temperatures, we found that lower temperatures led to later release (17 ± 1 days at 35 °C) while higher temperatures caused earlier release (12 ± 0 days at 39 °C) when compared to standard physiological temperature (14 ± 0 days at 37 °C) (Figure S7b, Supporting Information). These findings suggest that even a severe, extended fever is unlikely to meaningfully accelerate drug release.

To demonstrate the scalability of the PULSED method, a 22×14 array of open-faced cylinders were generated, filled, and sealed (Figure 3a-d). Incubating these microparticle arrays in PBS for 12 h under agitation at 37 °C showed a recovery that was only marginally above background at $0.05 \pm 0.03\%$ of the total filled contents, suggesting that sealing was highly consistent across the array. The signal observed is likely due to a few aberrant drops from the piezoelectric dispenser rather than inadequate sealing since the amount recovered is far less than

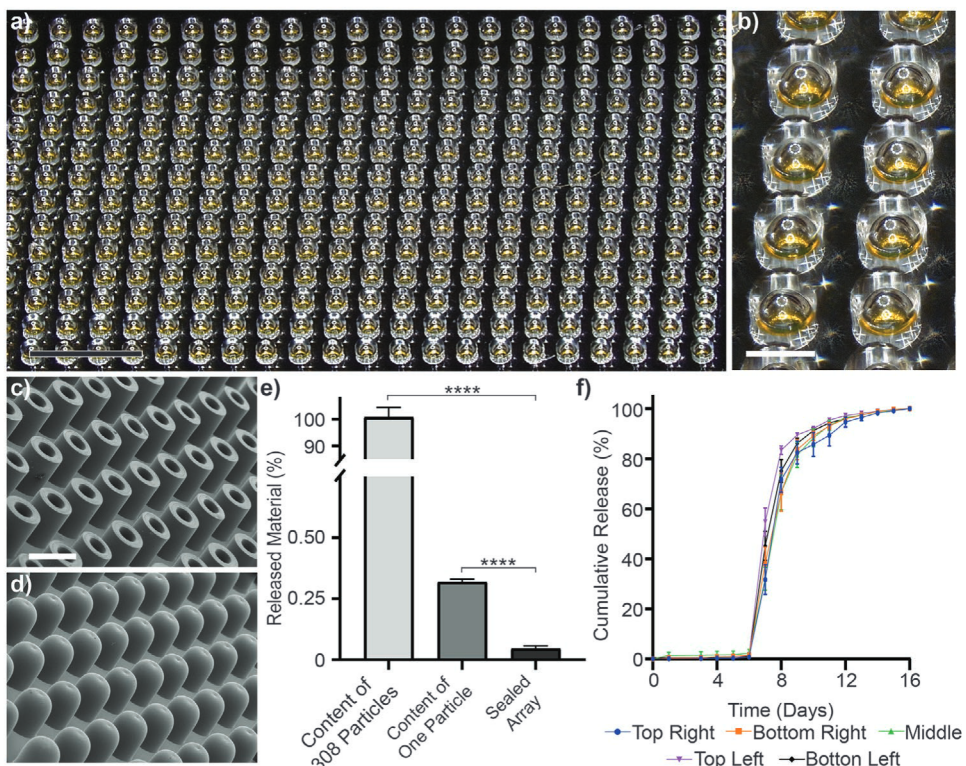


Figure 3. Scale-up of the PULSED microparticle fabrication method. Stereoscope images of a) the filled and sealed 22×14 particle array and b) a close-up of several particles within the array. All particles were composed of $\text{PLGA}_{13\text{COOH}}$ and filled with $1 \mu\text{g}$ of 10kDa fluorescein isothiocyanate-labeled dextran prior to sealing. SEM images of c) unsealed and d) sealed PULSED microparticles. e) Model drug recovered from a large array (22×14) of sealed $\text{PLGA}_{13\text{COOH}}$ microparticles compared to the contents of 1 and 308 particles ($n=3-5$). $****p < 0.0001$ was calculated using a one-way ANOVA with Tukey's multiple comparison test. f) In vitro cumulative release of fluorescein isothiocyanate-labeled 10kDa dextran from $\text{PLGA}_{13\text{COOH}}$ microparticles harvested from different regions (top-left, bottom-left, center, top-right, and bottom-right) of the microparticle array ($n=7$). Error bars indicate the standard error of the mean. Scale bars: white = $400 \mu\text{m}$, black = 2 mm .

the contents of even a single particle (Figure 3e). In order to validate the uniformity of sealed microparticle behavior, in vitro release studies were performed using particles harvested from five distinct regions of the large microparticle array. These studies showed excellent consistency with pulsatile release centered around day 8 ± 0 , 8 ± 1 , 8 ± 0 , 8 ± 1 , and 8 ± 1 for the top-left, bottom-left, center, top-right, and bottom-right regions of the array, respectively exhibiting no statistical difference in array location ($p > 0.05$) (Figure 3f). Finally, to assess throughput, we filled, sealed, and harvested sixteen 22×14 particle arrays containing a total of 4928 particles each filled with $3 \mu\text{g}$ of 10kDa dextran conjugated to fluorescein isothiocyanate in approximately 9 h and 34 min, corresponding to one particle created approximately every 7 s. Although inadequate for global commercial production with one operator at lab-scale production, this throughput can be immediately improved by using larger particle arrays and/or filling more arrays simultaneously. However, to enable a commercially viable process that meets the cost and throughput required to meet global needs, a continuous, automated process would likely be necessary. Fortunately, the PULSED method is well-suited for this transition since it does not require the complex alignment of components to fully encapsulate the payload.

Next, we sought to identify a simple method for expanding the library of particle compositions with different temporal

delays prior to release. We hypothesized that blending PLGA polymers with different properties could enable us to achieve intermediate time points. To test this hypothesis, we prepared a solution of $\text{PLGA}_{13\text{COOH}}$ and $\text{PGLA}_{87\text{COOR}}$ in an organic solvent, cast solid films using the blended polymer solution, and generated particles to evaluate in vitro release. Pure $\text{PLGA}_{13\text{COOH}}$ and $\text{PGLA}_{87\text{COOR}}$ particles prepared using this approach were released on days 6 ± 0 and 30 ± 0 while blends with approximate molar ratios of 12:1, 5:1, and 3:5 ($\text{PLGA}_{13\text{COOH}} : \text{PGLA}_{87\text{COOR}}$) exhibited release on days 9 ± 1 , 12 ± 0 , and 18 ± 0 , respectively, which supported our hypothesis (Figure S8, Supporting Information). Sharp pulsatile release kinetics were also maintained with over 75% of the model therapeutic, releasing within 2 days for all three blends. These results suggest a simple path forward for more extensive customization of the release delay.

Biotherapeutics (e.g., proteins) have rapidly emerged as an important pharmaceutical class due to their high specificity, functionality, and potency.^[43] In 2021, seven of the top ten best-selling drugs in the United States were biologics.^[44] However, biologics generally cannot be administered orally due to their low oral bioavailability and instead require repeated parenteral injections, which may require administration by a medical professional. Given that biotherapeutics are generally less stable than most small molecule drugs,^[45,46] we set out to determine the effects of the PULSED fabrication process on

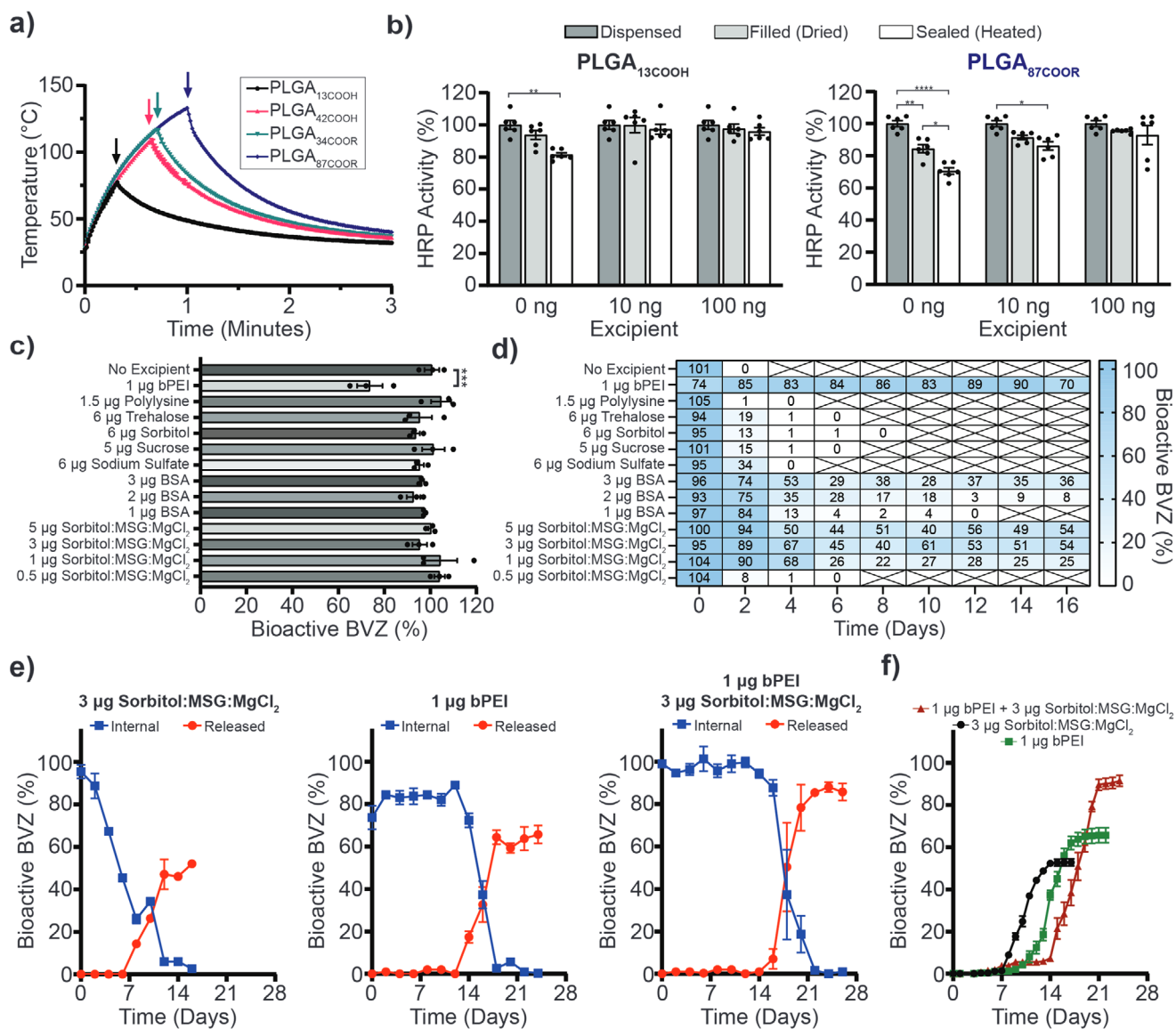


Figure 4. Heat exposure and protein stability during encapsulation and release. a) Graph of the temperatures experienced by microparticles during microparticle sealing for $\text{PLGA}_{13\text{COOH}}$, $\text{PLGA}_{42\text{COOH}}$, $\text{PLGA}_{34\text{COOR}}$, and $\text{PLGA}_{87\text{COOR}}$. Arrows indicate when particles were removed from the heat source ($n=3$). b) Graphs showing the retention of enzymatic activity of HRP in microparticles composed of $\text{PLGA}_{13\text{COOH}}$ and $\text{PLGA}_{87\text{COOR}}$ after filling and sealing with varying amounts of trehalose as a stabilizing excipient ($n=6$). Statistical analysis done using two-way ANOVA with Tukey's multiple comparison test. c) BVZ) bioactivity after drying and sealing in $\text{PLGA}_{13\text{COOH}}$ microparticles filled with various excipient formulations ($n=3$). Statistical analysis done using a one-way ANOVA with Dunnett's multiple comparisons test. d) Heat map showing the total bioactive BVZ (particle contents and released) encapsulated in $\text{PLGA}_{13\text{COOH}}$ and incubated at 37 °C ($n=3$). e) Data showing release kinetics and BVZ bioactivity ($n=3-12$). f) Cumulative release of bioactive BVZ released from $\text{PLGA}_{13\text{COOH}}$ microparticles with different stabilizing excipients ($n=11-12$). All stability data is normalized to the loading control. All error bars indicate standard error of the mean. * $p < 0.05$, ** $p < 0.01$, *** $p < 0.001$, **** $p < 0.0001$.

the bioactivity of an encapsulated protein. First, we measured the temperature at the microparticle interface during sealing to quantify the thermal stress that the biologic might experience (Figure 4a). $\text{PLGA}_{87\text{COOR}}$, the highest molecular weight polymer studied, took the longest amount of time to seal and therefore experienced the greatest thermal stress, momentarily reaching a temperature of 133 °C. In contrast, $\text{PLGA}_{13\text{COOH}}$ only reached a highest temperature of 77 °C. In general, we observed that PLGAs with higher molecular weights and ester end groups required longer sealing times.

Concerned that the microparticle preparation process might harm encapsulated biologics, we then created microparticles containing horseradish peroxidase (HRP), a model biologic,^[47,48] to assess protein bioactivity after the filling and sealing steps of the PULSED process, which could cause damage due to drying and heating, respectively. Drying and sealing were found to cause mild, yet significant reductions in HRP bioactivity when the enzyme was encapsulated in $\text{PLGA}_{13\text{COOH}}$ microparticles with no excipient, retaining 94.2 ± 6.9% enzymatic activity after sealing, and 81.4 ± 3.2% after incurring the thermal stress from

sealing. This drop in bioactivity was easily ameliorated with the addition of a small amount (10 ng) of trehalose, which increased the recovery of enzymatic activity to $97.3 \pm 7.5\%$ after drying and sealing. In comparison, PLGA₈₇COOR microparticles exhibited greater amounts of damage after drying ($85.8 \pm 6.0\%$ of initial bioactivity), which further decreased after sealing ($70.6 \pm 5.0\%$ bioactivity). Although 10 ng of excipient significantly improved HRP bioactivity after filling to $91.7 \pm 3.5\%$, 100 ng of trehalose was required to recover HRP bioactivity at levels that were not significantly different from the activity of the loading control at $100 \pm 6.9\%$ (Figure 4b). The reduced bioactivity of HRP after encapsulation in PLGA₈₇COOR relative to PLGA₁₃COOH is likely a result of increased heat exposure, but easily prevented using trehalose as a thermostabilizing excipient.

After showing the stabilization of a model protein with a convenient bioactivity readout through the microparticle fabrication process, we then sought to demonstrate the bioactivity of a clinically relevant therapeutic through encapsulation and release. Bevacizumab (BVZ), brand name Avastin, is a humanized monoclonal anti-vascular endothelial growth factor (VEGF) antibody that is FDA-approved as a therapeutic for several types of cancer and is prescribed off-label for neovascular age-related macular degeneration.^[49] Using PLGA₁₃COOH, we screened stabilizing excipients, including formulations previously reported to stabilize proteins in PLGA microspheres,^[50,51] to maximize the stability of BVZ through the PULSED fabrication process. Bioactivity was assessed using an enzyme-linked immunosorbent assay (ELISA) that relies on the antibody binding to its target, VEGF. BVZ without excipient was very stable through the filling and sealing processes in PLGA₁₃COOH microparticles as $101 \pm 5.3\%$ of bioactive BVZ was recovered, suggesting that the monoclonal antibody is more stable than HRP through particle fabrication. None of the excipients that we explored for subsequent stabilization (i.e., through the release process) significantly affected recovery through encapsulation relative to the no excipient control with the exception of branched polyethyleneimine (bPEI), which reduced the bioactivity of BVZ to $73.7 \pm 9.5\%$ of its initial activity after encapsulation (Figure 4c).

Next, we performed an in vitro release study to assess the stability BVZ encapsulated in PLGA₁₃COOH microparticles at 37°C . In these studies, particles were removed from incubation at 37°C on the designated day. Then the supernatant was removed to analyze BVZ released from particles, then particles were resuspended and crushed to release the contents of the particle's core. These samples were analyzed using an ELISA. Figure 4d shows a heat map of the total bioactivity of BVZ, which was measured as the sum of the bioactivity obtained from the supernatant surrounding particles and the amount harvested from within the particles. Without excipients, BVZ quickly loses its bioactivity with 0% remaining by day two. Most excipients tested failed to stabilize BVZ past six days, which is before the expected release date. Only formulations containing bovine serum albumin (BSA), sorbitol:monosodium glutamate (MSG):MgCl₂ (10:8.5:8.5 mass ratio), and bPEI retained bioactive BVZ through day 16. The BSA and sorbitol:MSG:MgCl₂ formulations exhibited dose-dependent stabilizing effects. In both cases, the bioactivity of BVZ significantly decreased in particles containing less than 3 μg of excipients. Although

BSA was able to stabilize BVZ to some extent ($35.6 \pm 12.7\%$ recovery), 3 μg sorbitol:MSG:MgCl₂ outperformed 3 μg of BSA, recovering $54.3 \pm 2.3\%$ of bioactivity on day 16. Interestingly, despite the initial loss in BVZ activity during encapsulation, bPEI largely prevented a reduction in bioactivity throughout release, resulting in $70.3 \pm 5.5\%$ on day 16, which was the highest of any formulation tested. This stabilizing effect may be due to bPEI's ability to act as a proton sponge, which could prevent a severe drop in pH that is typically caused by PLGA degradation into acidic by-products.^[52]

We then distinguished bioactive BVZ remaining inside the microparticle and the amount released at each time point in the two best-performing formulations containing 3 μg sorbitol:MSG:MgCl₂ and 1 μg bPEI (Figure 4e). The 3 μg sorbitol:MSG:MgCl₂ formulation supported the recovery of 95% BVZ bioactivity on day 0, but continually decreased until release began after day 6. In contrast, the 1 μg bPEI formulation largely prevented a decrease in BVZ activity while the antibody remained inside the particle, only losing some activity during the release process. In an attempt to further increase bioactivity the 3 μg sorbitol:MSG:MgCl₂ and 1 μg bPEI formulations were combined, resulting in $99.0 \pm 2.6\%$ of BVZ remaining stable through fabrication, and the release of $85.7 \pm 7.0\%$ of the monoclonal antibody measured on day 26. The enhanced recovery is likely due to different stabilization mechanisms. The sorbitol:MSG:MgCl₂ formulation appears to prevent the initial destabilization of bPEI during the fabrication process, while bPEI stabilizes the monoclonal antibody until release.

Finally, to quantify release kinetics in a single population of microparticles evaluated longitudinally, particles containing BVZ were incubated at 37°C and supernatant was routinely collected to measure bioactive antibody release. The 3 μg sorbitol:MSG:MgCl₂ formulation released most of its bioactive contents by day 10 ± 1 , resulting in a recovery of $52.8 \pm 5.7\%$ active BVZ. The 1 μg bPEI formulation resulted in a release of $65.7 \pm 12.3\%$ bioactive BVZ centered on day 14 ± 1 . Given the difference in release, it is apparent that the contents of PULSED microparticles can affect PLGA degradation. It is likely that the buffering effects of bPEI acted to prevent particle acidification, thereby mitigating the acid-catalyzed hydrolysis of PLGA and delaying release relative to non-buffered formulations. Combination of the top-performing excipient formulations, increased BVZ bioactivity to $91.5 \pm 9.0\%$ with release centered at 18 ± 2 days (Figure 4f). To continue exploring the clinical viability of this system, we evaluated the storage stability of BVZ-filled particles at 4°C in desiccant. After four weeks, negligible losses in BVZ bioactivity were observed (Figure S9, Supporting Information).

Although most small molecule drugs are not likely to require stabilizing excipients, these additives are required for all but the most robust of proteins.^[53] Even with excipients, it may be difficult to stabilize some therapeutics in the context of PUSLED microparticles due to stressors experienced during fabrication or during release. However, we anticipate that many other clinically impactful and top-selling antibodies other than BVZ could also be stabilized by using excipients to counteract key environmental stressors. The volume of each microparticle core is limited by a combination of needle diameter and microparticle wall thickness and therefore any volume occupied by excipients reduces the amount of the protein that

can be loaded. Nevertheless, very few particles may be required for some applications, such as vaccination. For example, the hepatitis A vaccine contains only 100 ng of viral antigen.^[54] If formulated into PULSED microparticles at a mass ratio of 40:1 excipients:vaccine, a single dose of the hepatitis A antigen could still be encapsulated in a single particle. The coadministration of several PULSED microparticles releasing at different time points separated by one month or more could then enable single-injection vaccination with fewer than 10 particles. Additionally, PULSED microparticles containing BVZ could be injected intraocularly to treat neovascular age-related macular degeneration, which requires only a few micrograms of antibodies to be present within the eye to prevent disease progression.^[55] By delivering BVZ in a controlled-release format, the frequency of intraocular injections required could be greatly reduced, thereby improving patient adherence.^[56]

After demonstrating the consistency, tunability, and versatility of the PULSED encapsulation method, we sought to develop a microparticle filling strategy that overcomes the limitations of piezoelectric filling. Although robotic piezoelectric picoliter dispensers are highly programmable, precise, and accurate, these tools have several key limitations. Namely, they dispense liquid in a serial manner, are incompatible with viscous solutions, and can be prohibitively expensive, limiting access to this technology and increasing microparticle production cost. To overcome these limitations, two additional fluid filling methods were explored—syringe pump filling and flood filling (Figure S10, Supporting Information). The first method uses a standard syringe pump with a custom 3D-printed adapter attached to tubing that narrows the fluid flow path to a diameter capable of fitting within the particle core. The flood-filling method uses vacuum and centrifugation to pull a solution into submerged particles in a batch-filling process.

To determine the predictability and consistency of drug loading into particles, we altered the filling concentration and/or the number of filling cycles for all three fluid filling methods. Changing the concentration of the filling solution was a reliable way of controlling the total amount of a material filled into the core using the piezoelectric and syringe pump methods showing a strong linear correlation, with R^2 values equal to 0.9920 and 0.9911, respectively. The flood fill method had a lower R^2 equal to 0.9684 and was generally more variable than the piezoelectric and syringe pump filling methods (Figure 5a and Figure S11a, Supporting Information). When the concentration of drug in the filling solution cannot be easily increased due to solubility or the viscosity constraints of the filling method, the solution can instead be dispensed at a viable concentration (i.e., viscosity) repeatedly into the same particle with intermittent delays that allow the previously dispensed solution to spontaneously evaporate, freeing up the volume for dispensing solution in the next filling cycle. This cyclic approach to filling particles with drug resulted in a high linear correlation with the amount of material filled with an R^2 equal to 0.9936 and 0.9902 for the piezoelectric and syringe pump filling methods, respectively. The amount recovered from the particle after employing the flood fill method increased linearly at low cycle numbers but appeared to plateau after 4 cycles ($R^2 = 0.5500$), suggesting that an equilibrium is reached where

the mass of drug entering the particles in each new filling cycle is equivalent to the mass being resolubilized and removed (Figure 5b and Figure S11b, Supporting Information).

With respect to commercial scale-up, dispensing higher-concentration solutions into particles is preferred over increasing cycle numbers because it requires less processing time; however, a key limitation of piezoelectric dispensing is its inability to dispense viscous solutions. If a solution is visually observed to be even slightly more viscous than water, it is unlikely to be compatible with most piezoelectric dispensing equipment. To determine if the viscosity limitations of the piezoelectric dispensing system could be overcome using the syringe pump or flood filling methods, we prepared carboxymethylcellulose (CMC) sodium salt solutions at different viscosities and determined their compatibility with filling. The piezoelectric dispensing method was able to dispense CMC solutions with viscosities as high as 5.6 cP, the flood filling method was able to dispense solutions as high as 178 cP, and the syringe pump method was able to dispense solutions with a maximum viscosity of 193 cP (the highest tested). Solution viscosities were determined at a shear rate of 200 s⁻¹ (Figure S12, Supporting Information). By offering compatibility with viscous solutions, the syringe pump methods are able to fill drugs at far higher concentrations, potentially reducing microparticle fabrication cost and increasing throughput. Flood filling offered more moderate gains in viscosity compatibility relative to piezoelectric dispensing, but could still be useful in cases where the drug is highly water-soluble and inexpensive since it enables batch (i.e., non-serialized) microparticle filling.

Next, since all liquid filling methods are ultimately limited by drug solubility, we explored a dry filling method, which consisted of packing solid lyophilized material that had assumed a compressible microfibrous structure into microparticle cores using a 34-gauge needle (Figure S10, Supporting Information). Although this filling approach is more time-intensive due to the manual nature of the current process, this method has utility for filling materials with extremely low water solubility. To demonstrate this principle, microparticles were filled with 0.28 ± 0.03 µg of imiquimod, a very hydrophobic drug. Aqueous filling approaches for imiquimod are impractical, requiring 11,200 cycles to fill the same amount of material due to imiquimod's low solubility in water (approximately 2 µg mL⁻¹).^[57] Finally, we confirmed each filling method was compatible with sealing and that the particles produced using these methods all exhibited pulsatile release kinetics that was not significantly different ($p = 0.37$) as determined using a two-way ANOVA (Figure 5c–e).

To further explore the capabilities and limitations of this fabrication method, we probed the effects of altering microparticle geometry on the sealing process. Although our original particles readily pass through an 18-gauge needle, which is routinely used for some applications, such as IV blood collection, smaller microparticles would enable the use of narrower needles and improve patient acceptability, especially in pediatric populations. Therefore, we created miniaturized particles that maintained the same ratio of height to diameter to wall thickness of 5:4:1 and loading capacity of ~8.6%. These particles were easily sealed (Figure 6a–d); however, due to the diameter of the smallest droplets created by the piezoelectric dispenser

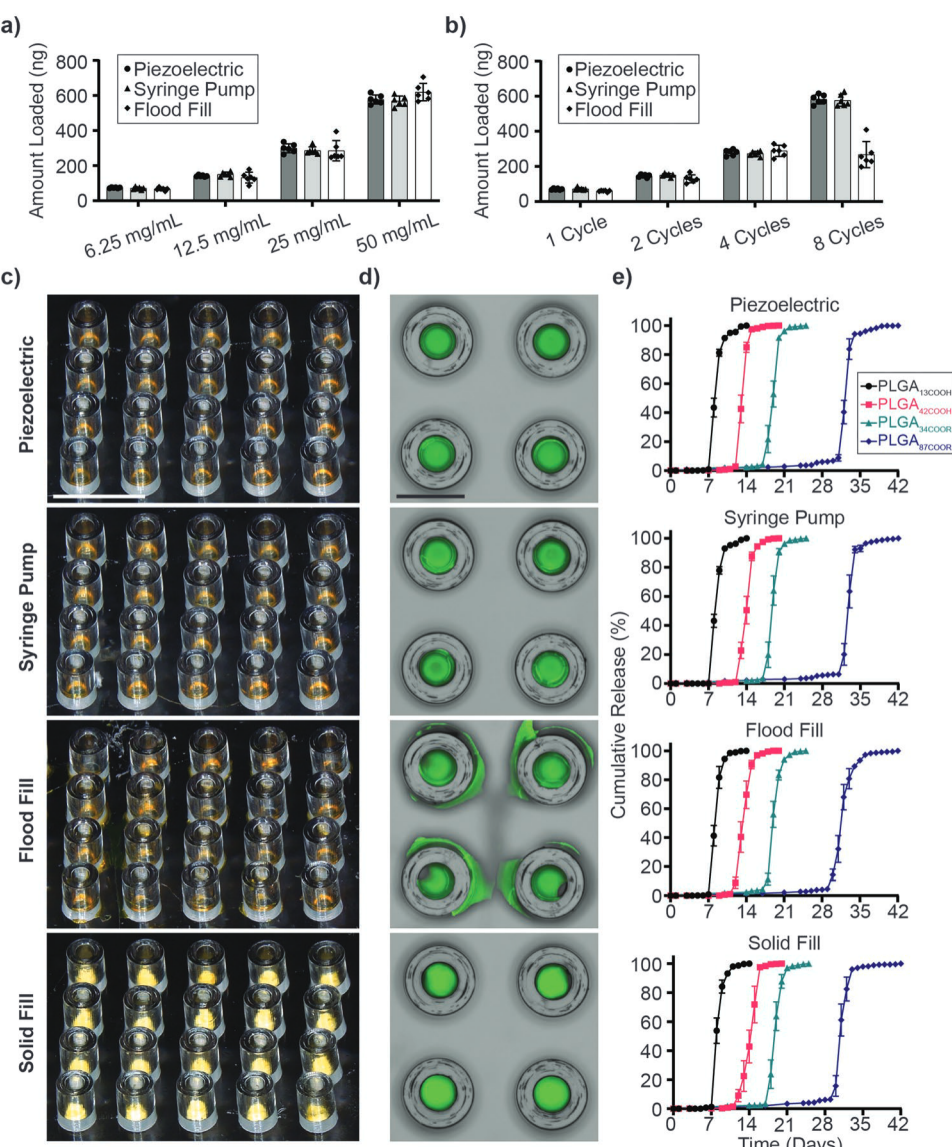


Figure 5. Evaluation of alternative microparticle filling methods. Graphs showing the amount of model drug filled into microparticles in response to increasing the a) solution concentration ($n=6$) or b) the number of cycles for various fluid filling methods ($n=6$). c) Stereoscopic and d) overlapped and fluorescence microscopy images of particles viewed from the side and top. e) Graphs showing the normalized release of 1 μ g fluorescein isothiocyanate-labeled 10 kDa dextran from PLGA microparticles filled using the piezoelectric dispenser, syringe pump, flood filling method, and solid filling method ($n=11-12$).

and its imperfect dispensing accuracy, it was not possible to reliably fill the solution into particles with an outer diameter of smaller than 300 μ m. To fill even smaller particles, different versions of the syringe pump adapter were 3D-printed to allow the tip to fit inside the core of the smaller particles. Using this loading technique, we were able to fill microparticles with an external diameter of 100 μ m, corresponding to approximately a 64-fold decrease in particle mass (Figure 6e–j). These particles were capable of freely flowing in a 30-gauge needle, which is smaller than the size used for most pediatric vaccinations (22 to 25 gauge), and on par with the smallest commonly used needles for insulin administration and intravitreal injections (29 to 31 gauge).

Next, we sought to alter the shape and aspect ratio of the particles, generating open-faced cylinders and rectangular prisms composed of PLGA_{13COOH} with varying heights and wall thicknesses (Figure S13, Supporting Information). Both types of microstructures appeared rounded after sealing, though cylindrical particles sealed more quickly than similarly dimensioned rectangular particles. Particle height also played a role in sealing time, with shorter particles—which are more distant from the hot plate surface—taking longer to seal, while the shortest rectangular particles did not seal, demonstrating particle height was critical for the creation of sealable particles. Finally, walls as thin as 50 μ m did not inhibit sealing or affect the sealing time for either geometry. The wall thickness is

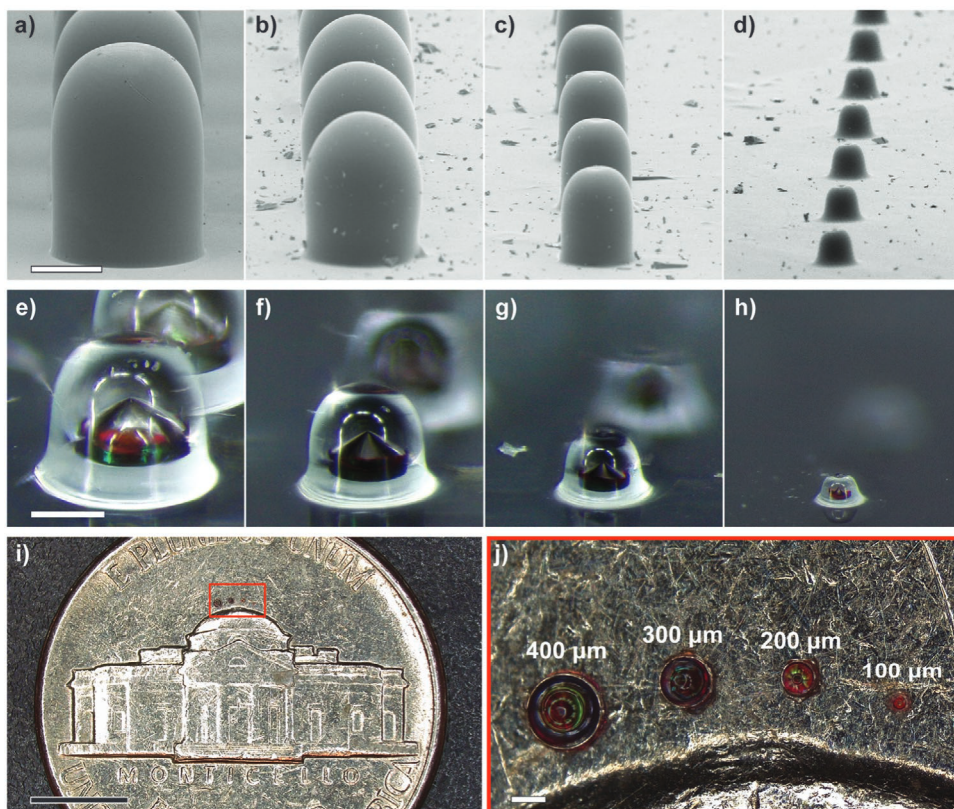


Figure 6. Miniaturization of PULSED microparticles. SEM images of PULSED particles with a diameter of a) 400, b) 300, c) 200, and d) 100 μm . Stereoscope images of PULSED particles with a diameter of e) 400, f) 300, g) 200, and h) 100 μm filled with a $120 \mu\text{g mL}^{-1}$ fluorescein sodium salt solution. i,j) Images of microparticles on a nickel for scale. Scale bars: black = 5 mm, white = 200 μm .

an interesting parameter that could be explored to increase particle loading capacity without altering the particles' outer dimensions, which can negatively impact injectability through small-diameter needles. These results show that not all geometries can be sealed using this strategy; however, geometries well-suited for injection, such as cylinders, are readily sealable.

Currently, SEAL is the existing “best-in-class” pulsatile microparticle delivery system, enabling rapid release of material at a predetermined time. We produced a cylindrical version of the SEAL process that has recently been reported^[58] to compare to PULSED microparticles. Although the outer appearance of microparticles produced by each method is different, both fabrication methods created particles that exhibited tunable delays and rapid release, with particles losing more than 75% of contents over four or fewer days for all PLGAs tested (Figure S14, Supporting Information). Although comparable to the SEAL process in release, the PULSED fabrication process offers several key advantages. Namely, it offers the ability easily produce large numbers of uniform microparticles, requires minimal skill to seal the particles, and is compatible with small particles to flow through needle gauges commonly used in the clinic. We further hypothesized that the contactless thermal sealing of PULSED microparticles would enable drug encapsulation within crystalline polymers, which is very difficult to achieve with the contact-based SEAL process due to the combination of compression and the rapid transition of the polymer from a solid to a liquid.

We explored the ability of the PULSED process to seal particles composed of crystalline polymers using polycaprolactone (PCL), a crystalline polymer with a melting point of approximately 60 °C, as a model material. PCL microparticles sealed using the PULSED process exhibited morphology similar to that of PLGA particles formed using the PULSED method (Figure S15a-d and Video S2, Supporting Information). Additionally, the time window over which PCL particles were sealed and retained the appropriate morphology for encapsulation was approximately 10 s, providing a large margin for error and aiding in batch-to-batch consistency. Due to the rapid transition of PCL from a solid to a liquid at 60 °C, the cumulative thermal exposure of these particles is far lower than for PLGA, which begins to flow slowly when heated above its glass transition temperature. The base of the PCL particle never reached a temperature greater than 60 °C and only experienced temperatures over 50 °C for 1 min and 12 s. The lower thermal stress resulted in a recovery of $94.4 \pm 7.0\%$ HRP activity through the PULSED fabrication process when no excipients were used (Figure S15 e,f, Supporting Information) as compared to a recovery of $81.4 \pm 3.2\%$ HRP activity for PLGA₁₃COOH with a reported glass transition temperature of 42–46 °C. Although PCL has not been as-well studied in the context of drug delivery or utilized clinically to the extent that PLGA has, the slow degradation of PCL, which can take years *in vivo*, makes it a potentially attractive polymer to use for long-term drug delivery applications, such as vaccination.^[59]

3. Conclusion

In summary, the PULSED microparticle fabrication method, in combination with an adapted syringe pump filling method, enables the scalable production of small, fully biodegradable microparticles that exhibit pulsatile release after a customizable, material-dependent delay. This facile, one-component fabrication method consists of simple processing steps with the potential for automation without relying on highly specialized and expensive equipment. Further, its compatibility with proteins and low cost offers exciting potential for use in a broad array of applications ranging from the delivery of small molecule drugs to biologic therapeutics and prophylactics.

4. Experimental Section

Master Mold Generation: Particles were designed using the computer-aided design (CAD) software SolidWorks 2020 (Dassault Systems SolidWorks Corporation, Concord, NH, USA). STL files were converted to a file compatible with the Nanoscribe Photonic Professional GT laser lithography system (Nanoscribe GmbH, Karlsruhe, Germany) using Describe. Microparticle arrays were printed using the 10x objective and IP-Q photoresist on a treated silicon wafer. Briefly, substrates were cleaned, plasma treated with oxygen, and submerged in a 3-(trimethoxysilyl)propyl methacrylate (1% v/v) ethanol solution for 12 h. This treatment enhanced print adhesion to the substrate and was previously described elsewhere.^[60]

3D-printed microparticle arrays were developed in propylene glycol methyl ether acetate (PGMEA) for 45 min and then in isopropyl alcohol for 5 min to remove unpolymerized material. Arrays were then cured in a CL-1000 Ultraviolet Crosslinker ultraviolet light oven (Analytik Jena LCC, Upland, CA, USA) for 3 h or until features appeared yellow. Unless otherwise stated, open-faced cylinders were printed with an outer diameter of 400 μm , height of 500 μm , and wall thickness of 100 μm . All print recipes and CAD files are available upon request.

Inverse Mold Replication: Particle arrays were coated in a thin layer of trichloro(1H,1H,2H,2H-perfluoroctyl) silane (40 μL) (Sigma-Aldrich, St Louis, MO, USA) by placing the compound in a chamber under vacuum letting it passively evaporate and deposit on particle arrays over 1 h. Inverse molds with depressions rather than microparticle protrusions were then produced using soft lithography. Briefly, Sylgard 184 PDMS (Dow Corning, Midland, MI, USA) was prepared 9:1 (base:curing agent) mixed thoroughly, and centrifuged for 3 min at 300 rcf to remove bubbles. The PDMS solution was poured onto the primary or replicate particle arrays and degassed for 1 h. After 800 μm Teflon spacers (McMaster-Carr, Elmhurst, IL, USA) were placed at the edges of the particle arrays, a clean microscope slide was overlayed onto them. This structure was clamped with binder clips and placed in the oven at 120 °C for at least 6 h. After the structure was demolded to generate the inverse particle arrays (Figure S1a–c,g–i, Supporting Information).

Mold Replication: To promote separation, PDMS molds made from the original 3D-printed arrays were placed under vacuum with Trichloro(1H,1H,2H,2H-perfluoroctyl) silane (40 μL) for 1 h. Norland Optical Adhesive (NOA) 86H (Norland Products, Cranbury, NJ, USA), a photocrosslinkable polymer, was poured onto the PDMS inverse molds and pulled into the microfeatures under vacuum for 10 min, after which excess bubbles were removed using compressed air. This process was repeated a total of three times. A clean microscope slide was then overlaid onto the degassed NOA and a small 0.75-inch plastic spring clamp was used to hold the structure together. This assembly was left at room temperature for 30 min to allow for displacement of excess NOA, then placed in the oven at 120 °C for at least 12 h to allow adhesion of the NOA to the glass slide to fully mature. After, PDMS was demolded (Figure S1d–f, Supporting Information). Note that because NOA H86

was light sensitive, uncured adhesive was protected from light during all steps performed before it was placed in the oven. Note for alternative particle geometries generated in Figure S13, Supporting Information, this step was skipped and PDMS molds made from the master mold were directly used to generate PLGA particles.

Polymer Film Preparation: PLGA films were generated through compression molding of PLGA above its glass transition temperature. PLGA (\approx 420 mg) was placed on a Teflon sheet inside two 100 μm ring shims. An additional Teflon sheet was overlaid on top of the PLGA and clamped between two aluminum blocks using a c-clamp. The clamp was placed in an oven set at 120 °C for 1 h under vacuum. During this time the clamp was tightened until firm after 30 min of heating when PLGA was above its glass transition temperature. The assembly was then removed and placed in a desiccator to cool to room temperature. Once cool the PLGA films were readily removed from the Teflon. PCL with a M_w of 14 kDa (Sigma-Aldrich, St Louis, MO, USA) was used to make films in the same manner.

Experiments consisting of PLGA mixtures were generated using a solvent casing system to ensure homogenous mixing. PLGA was weighed out based on a molar ratio and used to prepare a 40% (w/v) solution in acetone. The solution was pipetted onto a Teflon sheet, attached to a double-wide glass slide, and passed under a doctor blade 500 μm higher than the Teflon. To remove organic solvent, films were placed on a hot plate at 40 °C for 6 h then placed under vacuum and 40 °C overnight. All films were stored in a desiccator until use.

Polymeric Microparticle Array Fabrication: PLGA particles were generated using PDMS molds. First, molds were coated with a thin layer of trichloro(1H,1H,2H,2H-perfluoroctyl) silane as described above. Next, PLGA films were placed on top of the micropatterned PDMS mold. A clean glass slide was laid on top and the two pieces were clamped together with 1-inch plastic spring clamps. This assembly was placed in an oven at 120 °C under vacuum. PLGA_{13COOH} was placed in the oven for 1 h, while PGLA_{42COOH}, PGLA_{34COOR}, and PGLA_{87COOR} were placed in the oven for 12 h. PCL was placed in the oven for 10 min due to its low melting point. After the clamps were removed and the components were allowed to cool to room temperature and the mold was separated resulting in PLGA or PCL microparticles attached to glass slides. Particle arrays were then stored in a desiccator until needed.

Microparticle Sealing and Harvesting: Arrays of PULSED microparticles were sealed using a custom 3D-printed holder printed with clear resin on a Form 2 3D printer (Formlabs, Sommerville, MA, USA). CAD files are available upon request. Cylindrical particles were inverted and placed 1 mm above a level stainless-steel block resting on a hotplate, with the particles facing the heat source. PLGA particles were sealed for varying durations over a level surface heated to approximately 200 °C while PCL was sealed using a surface temperature of approximately 74 °C as read by a thermocouple. Sealing times for PLGA_{13COOH}, PGLA_{42COOH}, PGLA_{34COOR}, and PGLA_{87COOR} were 18, 38, 42, and 60 s respectively, while PCL was sealed for 110 s. It was important to note that large amounts of payload material that accumulate on or near the tops of microstructures prevented proper sealing via the PULSED method. This was typically due to technical issues such as misalignment during piezoelectric filling, or poor packing during solid filling. Proper sealing material should be in the lower portion of the core, as seen in Figure 1d. Although not reported, it was also worth mentioning that open-faced cylinders can be sealed at various time and temperature combinations. Once removed from the heat source, particle arrays were placed 1 mm above a level lab bench with particles facing down and allowed to cool for 2 min. Afterward, single particles were harvested from the glass slide using a scalpel with a #12 blade, while entire arrays of particles were harvested using a razor blade.

To compare the particles produced using the PULSED method to those using the SEAL method, arrays of microparticle bases and caps were manufactured similarly to those described for PULSED particles. These particles were sealed by aligning cap and base components under a stereoscope and placing in direct contact with a hot plate at 65 °C as read by a thermocouple for various amounts of time. SEAL microparticles bases were made with an outer diameter of 400 μm ,

height of 275 μm , and wall thickness of 100 μm , while caps had a diameter of 400 μm , and height of 100 μm .

Piezoelectric Filling: A SciFLEXARRAYER S3 picoliter dispensing apparatus (SCIENION, Phoenix, AZ) equipped with an uncoated SCIENION PDC-80 tip was used to fill particles with fluorescein isothiocyanate-labeled 10 kDa dextran (3 μg) (Sigma-Aldrich, St Louis, MO, USA) dissolved in ultrapure water (30 mg mL $^{-1}$) or Alexa Fluor 647-labeled 10 kDa dextran (3 μg) dissolved in ultrapure water (10 mg mL $^{-1}$) unless otherwise specified. Particles were filled to the desired amount by varying the drop size, the number of drops per cycle, and the number of filling cycles. The amount actually dispensed from the piezoelectric nozzle was determined empirically and ranged from 65% to 85% depending on the solution. Fiducial marks were used to facilitate filling alignment.

Solid Filling: Fluorescein isothiocyanate-labeled 10 kDa dextran dissolved in ultrapure water (333 μg mL $^{-1}$) was aliquoted into polymerase chain reaction tubes (3 μL). Tubes were placed in a -80 °C freezer for 1 h and then lyophilized overnight. The resulting fibrous material was removed with a 34-gauge needle (Hamilton Company, Reno, NV, USA) and mechanically compressed into the cores of microparticles under stereoscopic guidance.

Imiquimod solid filling material was prepared by creating a solution of ≈450 kDa dextran (320 μg mL $^{-1}$) and imiquimod (40 μg mL $^{-1}$) dissolved in water (pH 1.9) adjusted with hydrochloric acid. The solution (12.5 μL) was aliquoted into polymerase chain reaction tubes, frozen with liquid nitrogen, and lyophilized overnight. The material was packed into particles, then four particles were dissolved in dimethyl sulfoxide (100 μL) and absorbance of 325 nm was read using Cary 60 UV-vis spectrophotometer (Agilent Technologies, Santa Clara, CA, USA). The amount of material in lyophilized polymerase reaction tubes was determined by dissolving the contents of four tubes in dimethyl sulfoxide (100 μL) and measuring absorbance.

Flood Filling: Arrays of 24 microparticles were submerged with fluorescein isothiocyanate-labeled 10 kDa dextran dissolved in ultrapure water (9 μL 80 mg mL $^{-1}$) for all experiments unless otherwise noted. A clean glass slide was clamped over the array on 400 μm spacers using binder clips to prevent rapid evaporation. The apparatus was placed under vacuum for 3 min. After the cover glass slide was removed, excess filling solution was wicked away using a Kim Wipe, and the array was centrifuged at 10 rcf for 5 min.

Syringe Pump Filling: A custom syringe pump adapter was first designed in SolidWorks and then fabricated using a Photonic Professional GT2 laser lithography system with the 10x lens and IP-Q resin and developed as described above. The syringe pump adapters used to fill miniaturized microparticles were developed in PGMEA for 12 h and then moved to fresh PGMEA for an additional 12 h. Afterwards, adapters were placed in isopropyl alcohol for 16 h and cured under an ultraviolet oven as described above. Filling adapters were attached to Tygon ND-100-80, 0.010" inner diameter x 0.030" outer diameter Masterflex microbore transfer tubing (Cole-Parmer, Vernon Hills, IL). The other end of the tubing was attached to a 30-gauge blunt needle affixed to a 1 mL syringe. The custom syringe pump adapters could also have been produced by commercial entities as a fee-for-service for those without access to a high-resolution 3D printer. A NE-1000 programmable syringe pump set between 0 and 0.010 mL h $^{-1}$ was used to fill particles. Particles were filled with fluorescein isothiocyanate-labeled 10 kDa dextran (1 μg) dissolved in ultrapure water (26.7 mg mL $^{-1}$) unless otherwise stated. Filling was conducted under a stereoscope.

Release Kinetics: All particles used to evaluate in vitro release kinetics were filled using the piezoelectric dispensing apparatus unless otherwise noted. Sealed particles were placed in 0.5 mL centrifuge tubes and washed 3 times with PBS (120 μL) to remove any filling material on the surface of the particles. PBS (120 μL) was added to each tube and incubated at 37 °C on an orbital shaker (100 rpm). In some studies, the incubation temperature was altered to 35 or 39 °C, while in others the pH was altered to 6.5, 6, and 4 by altering the pH of PBS using 6N HCl (Fisher Scientific, Waltham, MA). After a brief centrifugation to consolidate solution, the supernatant was collected and replaced with

fresh PBS on day 0, day 1, twice a week during the period release was not expected, and then daily beginning shortly before the expected release. Model drug release was measured by detecting fluorescence of the supernatant in a black, flat-bottom 96-well plate at 490/525 nm (ex/em) using a Tecan Infinite M200 microplate reader (Tecan Group Ltd., Männedorf, Switzerland). Particles that were released on day 1 were excluded from the study as they were either improperly sealed or damaged during harvesting.

For *in vivo* release studies, particles loaded with Alexa Fluor 647-labeled 10 kDa dextran (1 μg) were filled using the piezoelectric dispenser and sealed using the PULSED method then sterilized with three 70% ethanol washes. Particles were injected in a sterile CMC solution (2% w/v). This viscous solution enhanced particle flow. A single microparticle was pulled up into a 19-gauge filter needle (BD, Franklin Lakes, NJ, USA) and then injected subcutaneously into the left of SKH1-Elite hairless mice (CrI:SKH1-HR $^{h^+}$). In the right flank 20 microparticles were injected, 5 of each PLGA type (PLGA_{13COOH}, PGLA_{42COOH}, PGLA_{34COOR}, and PGLA_{87COOR}) where only one type of PLGA was filled with (1 μg) of Alexa Fluor 647-labeled 10 kDa dextran, while the other PLGA types remained empty. This experiment is shown graphically in Figure S6, Supporting Information. Release was measured using an IVIS Spectrum small animal imager (PerkinElmer, Waltham, MA). Images were taken using an exposure time set to auto, F/Stop of 2, excitation filter of 640 nm, and emission filter of 700 nm. Mice were anesthetized during both injection and imaging with isoflurane (2.5%) and placed on a platform heated to 37 °C. Release kinetics were then quantified using Living Image software (PerkinElmer, Hopkinton, MA) by drawing a region of interest around the injected particle and measuring the average radiant efficiency. All animal work was approved by Rice University's Institutional Animal Care and Use Committee (PHS/OLAW Assurance D16-00005, AAALAC 001676) under protocol number IACUC-20-065.

In vivo release kinetics were validated using a PerkinElmer IVIS Kinetic III small animal imager (PerkinElmer, Waltham, MA). PLGA particles filled with Alexa Fluor 647-labeled 10 kDa dextran (1 μg) using the piezoelectric dispensing or remaining unfilled were sealed, harvested, and added to a black, flat-bottom 96-well plate with 1 particle per well. Each well was filled with PBS (200 μL) and the microplate was covered using an adhesive plate sealing film. The microplates were then incubated at 37 °C on an orbital shaker (100 rpm). Before imaging, microplates were briefly centrifuged to consolidate the solution at the bottom of the plate and the adhesive plate sealing film was removed. Microplates were imaged using the IVIS. Images were taken using an exposure time set to auto, F/Stop of 2, excitation filter of 640 nm, and emission filter of 710 nm. After imaging, a fresh adhesive plate sealing film was applied to the microplate prior to being placed back in the 37 °C incubator under agitation (100 rpm). Release kinetics were then quantified using Living Image software by drawing a uniform region of interest around each microplate well of interest to measure the average radiant efficiency. Cumulative release data was normalized to the maximum amount of signal measured for each particle.

Data for both *in vitro* and *in vivo* release kinetics were reported as the day on which the particle was released and the time span over which a particle releases 75% or more of its total contents. The day of release was defined as the day at which the cumulative release from an individual particle surpassed half of its total contents. The time span of 75% release was defined as the shortest span of consecutive days needed for an individual particle to release 75% or more of its contents. All values were rounded to the nearest whole numbers to match the maximum temporal frequency of sampling during the release experiments.

Microparticle Imaging: Stereoscope images were taken using a Leica S9i microscope (Leica Camera, Wetzlar, Germany). The resulting images were focus stacked using helicon focus 7 software (HeliconSoft, Kharkiv, Ukraine) to enable robust 3D imaging. SEM images were taken using a Thermo Fisher Apreo scanning electron microscope or a Phenom XL Desktop scanning electron microscope (Thermo Fisher Scientific, Waltham, MA).

Polymer Properties: The molecular weight and polydispersity index of stock PLGA polymers were determined using gel permeation

chromatography with an Agilent 1260 Infinity II System (Agilent, Santa Clara, CA). This consisted of two columns in series (PL113-6300), an isocratic pump (G7001B), column thermostat (G7116A), vial sampler (G7921A), and a multi-detector system (G7800A) with a refractive index detector, dual-angle light scattering detector, and viscometer. Samples were prepared in tetrahydrofuran (4 mg mL^{-1}) and filtered through a $0.22 \mu\text{m}$ membrane. The samples were run at 35°C at a flow rate of 1 mL min^{-1} under isocratic conditions. Agilent GPC/SEC Software was used to control the system and analyze data.

Viscosity Studies: To determine the most viscous solution that could be filled using each of the filling methods the following fourteen CMC sodium salt $n = 500$ (Tokyo Chemical Industry, Tokyo Japan) solutions were made: 5%, 4.5%, 4%, 3.5%, 3%, 2.5%, 2%, 1.5%, 1%, 0.75%, 0.5%, 0.25%, 0.125%, and 0.0625% (w/v). These solutions were used to fill open-faced cylinders until they failed due to increased viscosity. The piezoelectric dispensing unit failed when stable drops would no longer dispense, syringe pump filling failed when the 3D-printed syringe pump attachment was dislodged from the attached tubing, and the flood fill method failed when the solution was unable to be consistently pulled into particle cores under vacuum.

Viscosity measurements of CMC solutions were collected on a Discovery Hybrid Rheometer (TA Instruments, New Castle, Delaware, USA) equipped with a 40 mm diameter solvent trap-equipped stainless steel parallel plate geometry set to a gap height of $400 \mu\text{m}$. The sample ($550 \mu\text{L}$) was plated on the stage heated to 25°C , and a shear rate ramp from $10\text{--}500 \text{ s}^{-1}$ was used to determine the viscosity as a function of shear rate. The apparent viscosity was reported at a shear rate of 200 s^{-1} .

Sealing Efficiency: Fluorescein isothiocyanate-labeled 10 kDa dextran ($1 \mu\text{g}$) was filled into 1 or 308 microparticles using the piezoelectric dispensing machine. Particles were then sealed using the PULSED method as previously described. The glass slides containing the particle array were carefully trimmed using a diamond pen and placed inside a 50 mL Falcon tube containing PBS (5 mL). To promote leakage from unsealed particles arrays were placed under vacuum for 3 min, then left to agitate on an orbital shaker (100 rpm) for 12 h at 37°C . A standard curve of encapsulated material was generated by filling 22×14 microstructure arrays with 0, 1, 2, 4, 8, or 16 particles ($n = 3$) with fluorescein isothiocyanate-labeled 10 kDa dextran ($1 \mu\text{g}$). Arrays were then sealed, trimmed with a diamond pen, and placed in PBS (5 mL). Particles were then cut open using a scalpel. Note the 308 particle contents shown in Figure 3e were extrapolated from the 16-particle standard by multiplying values to reflect a full 308-particle array.

Excipient Filling: PLGA microparticles were first filled with excipients using the piezoelectric dispenser. The excipients and dispensing concentrations were as follows: branched polyethyleneimine with a M_w of 25 kDa (10 mg mL^{-1}), poly-L-lysine with a M_w of 150 to 300 kDa (2.5 mg mL^{-1}), D-Sorbitol (100 mg mL^{-1}), magnesium chloride, sodium sulfate (50 mg mL^{-1}), monosodium glutamate (Sigma-Aldrich, St Louis, MO, USA), D-sucrose (100 mg mL^{-1}), bovine serum albumin (15 mg mL^{-1}) (Fisher Scientific, Waltham, MA), and D-trehalose (10 mg mL^{-1} or 100 mg mL^{-1}) (Tokyo Chemical Industry, Tokyo Japan). The sorbitol:MSG:MgCl₂ solution was dispensed as a single solution (37 mg mL^{-1} , 31.5 mg mL^{-1} , 31.5 mg mL^{-1}).

HRP Stability: Particles with or without trehalose were filled with Pierce Horseradish Peroxidase (10 ng , 2 mg mL^{-1}) (Thermo Fisher Scientific, Waltham, MA). A subset of particles was harvested after filling but prior to sealing to determine damage by drying and placed in Protein LoBind Eppendorf tubes containing PBS (1 mL). The remaining particles were sealed using the PULSED method and then harvested into tubes containing PBS (1 mL) and cut open. HRP loading was determined by dispensing the solution directly into a 1.5 mL Protein LoBind Eppendorf tubes containing PBS (1 mL). Tubes were placed under vacuum for 3 min to remove air from particle cores, thoroughly vortexed, then left on an orbital shaker for 1 h. To test enzymatic activity, samples ($100 \mu\text{L}$) were placed in wells of a transparent 96-well plate and mixed with SureBlue TMB 1 ($100 \mu\text{L}$) (Seracare Life Sciences Inc., Milford, MA, USA), which contains the components necessary for the enzymatic reaction to occur. This colorimetric reaction was stopped after 60 s by adding sulfuric acid

($100 \mu\text{L}$, 0.1 M). Plates were read using a Tecan Infinite M200 microplate reader measuring absorbance at 450 nm and a reference wavelength of 655 nm . Data were processed by interpolating values against a linear regression on the standards. Data was converted from concentration to mass and normalized to a filling control.

Bevacizumab Stability: PLGA_{13COOH} particles with or without previously filled excipients were further filled with BVZ (10 ng) (Selleckchem, Houston, TX) using the piezoelectric dispenser (10 ng , 3.3 mg mL^{-1}). Particles filled and sealed were harvested to determine damage due to drying and sealing. These particles were then placed in Protein LoBind Eppendorf tubes containing PBS with 0.2% BSA (0.7 mL) and broken open using a scalpel. BVZ loading was determined by dispensing the solution directly into a 1.5 mL Protein LoBind Eppendorf tubes containing PBS 0.2% BSA (0.7 mL).

In vitro release studies were then performed to assess BVZ bioactivity. Bioactive BVZ released from and within PLGA_{13COOH} particles was assessed by adding particles to 1.5 mL Protein LoBind Eppendorf tubes containing PBS 0.2% BSA (0.7 mL) and placed in a 37°C incubator on an orbital shaker (100 rpm) with enough tubes to terminally collect three samples per time point. Every two days, three tubes were removed from incubation, and the supernatant, containing released BVZ, was removed and placed into a fresh 1.5 mL Protein LoBind Eppendorf tube. Fresh PBS 0.2% BSA (0.7 mL) was replaced into the tube containing the particle, which was then crushed under a stereoscope using a scalpel to release any BVZ remaining in the particle. These samples were stored at 4°C for up to one week before analysis using an ELISA.

To determine BVZ release kinetics from PULSED particles longitudinally in a nondestructive manner, filled and sealed PLGA_{13COOH} particles containing the top three excipient formulations ($3 \mu\text{g}$ of Sorbitol:MSG:MgCl₂, $1 \mu\text{g}$ bPEI, and a combination of $3 \mu\text{g}$ of Sorbitol:MSG:MgCl₂ and $1 \mu\text{g}$ bPEI) and BVZ were placed in 1.5 mL Protein LoBind Eppendorf tubes (1 particle per tube) and incubated in PBS 0.2% BSA (0.7 mL) at 37°C on an orbital shaker (100 rpm). Particle supernatant was removed and then replenished with fresh PBS 0.2% BSA (0.7 mL) daily near the period of expected release. The collected supernatant samples were then stored in a 1.5 mL Protein LoBind Eppendorf tube at 4°C until they could be analyzed using an ELISA to determine the release of BVZ from the particles.

To test bioactivity, samples were analyzed using an ELISA. The ELISA method was based on a previously published method.^[61] Recombinant human VEGF₁₆₅ (PeproTech, Cranbury, NJ) was used to coat Maxisorb plates (Nunc, Roskilde, Denmark) by diluting the protein ($0.03125 \mu\text{g mL}^{-1}$) in a carbonate-bicarbonate buffer (50 mM, 9.6 pH). Solution was added to each well ($100 \mu\text{L}$) and then the plate was covered using an adhesive sealing film and incubated overnight at 4°C on an orbital shaker (100 rpm). The next day, plates were washed three times with a solution of PBS with 0.5% tween-20 (PBST), then blocked using a 2% BSA solution in PBST (350 μL per well). Plates were covered and incubated at 4°C for 1.5 h on an orbital shaker (100 rpm). Next, the liquid in plates was removed and samples were added to each well ($100 \mu\text{L}$), then covered with an adhesive sealing film and left at 37°C for 1.5 h on an orbital shaker (100 rpm). Plates were washed three times with PBST, then rabbit anti-human IgG conjugated to HRP was diluted 1:10 000 in a solution of 0.2% BSA in PBST and the solution was added to each well ($100 \mu\text{L}$), and plates were incubated at 37°C of 1.5 h on an orbital shaker (100 rpm). Finally, plates were washed five times with PBST and SureBlue TMB was added to each well ($100 \mu\text{L}$) before immediately covering them with aluminum foil. Plates were allowed to develop for 90–120 s before the reaction was terminated by adding 0.1 M sulfuric acid to each well ($100 \mu\text{L}$). Plates were read with a microplate reader measuring absorbance at 450 nm and a reference wavelength of 640 nm . Data was processed in GraphPad Prism 9 (GraphPad Software, San Diego, California, USA) by using a sigmoidal 4PL non-linear regression on the standards and then interpolating sample values. Data was converted from concentration to mass and normalized to a filling control except for samples used to determine shelf stability, which was normalized to day zero.

Statistical Analysis: Cumulative in vitro release from particles containing fluorescent dye was normalized to the total release measured for each particle. Statistical analysis of sealing efficiency ($n = 3\text{--}5$) and particle consistency across distinct regions of a 22×14 was calculated using a one-way ANOVA with Tukey's multiple comparison test ($n = 7$). A two-way ANOVA was utilized to determine if the filling method influenced release kinetics ($n = 11\text{--}12$).

Cumulative release of fluorescent dye in vivo was normalized to the maximum amount of signal measured from each particle at any time point. Days after the point of the highest measured signal for each particle were reported as 100% to avoid artifacts associated with the slow decrease in fluorescence that occurs as already-released Alexa Fluor 647-labeled dextran was cleared from the surrounding area. A two-way ANOVA was used to determine the effect of number of particles injected on release.

To determine the stability of biologics (HRP and BVZ) through the sealing process and release, data was normalized to the amount of material initially dispensed into particles. To determine the damage done to HRP due to drying and sealing ($n = 6$), a two-way ANOVA with a Tukey's multiple comparison test was used. A one-way ANOVA using Dunnett's multiple comparisons test was utilized to determine statistical significance in BVZ stability relative to the no excipient control ($n = 3$).

Results were determined to be significant if $p < 0.05$. All error bars shown in figures represent the standard error of the mean, while standard deviation was reported in the body of the text. All statistical analysis and graphing done in this paper were done using GraphPad Prism 9.

Supporting Information

Supporting Information is available from the Wiley Online Library or from the author.

Acknowledgements

This work was supported in full (100%) by public funding from the Cancer Prevention and Research Institute of Texas (Grant No. RRI190056) and the National Institutes of Health (R03 EB031495). The authors also acknowledge the support of Rice University's Biomaterials Lab, which was supported in part by NIH (P41 EB023833). The content was solely the responsibility of the authors and does not necessarily represent the official views of the National Institutes of Health. B.H.P. (Grant No. 1842494) and T.B. (Grant No. 2236422) were supported by the National Science Foundation Graduate Research Fellowship Program. The authors would like to acknowledge the generosity of Rebecca Richards-Kortum for allowing the use of her SciFLEXARRAYER S3 picoliter dispensing apparatus as well as Dr. Chelsey Smith for her instruction on using the device. The authors would also like to acknowledge the Shared Equipment Authority at Rice University, specifically Jing Guo, James Kerwin, and Tim Gilheart.

Conflict of Interest

The authors currently have a provisional patent filed based on the encompassed work.

Data Availability Statement

The data that support the findings of this study are available from the corresponding author upon reasonable request.

Keywords

controlled release, drug delivery, high-throughput formulation, microparticle fabrication, pulsatile release

Received: January 8, 2023

Revised: February 20, 2023

Published online: March 30, 2023

- [1] C. B. Martin, C. M. Hales, Q. Gu, C. L. Ogden, *Prescription Drug Use in the United States, 2015–2016*, National Center for Health Statistics, Hyattsville, MD **2019**.
- [2] M. Aitken, M. Kleinrock, *Global Medicines Use in 2020: Outlook and Implications*, IMS Institute for Healthcare Informatics, Parsippany, NJ **2015**.
- [3] R. S. Festa, M. H. Tamaroff, F. Chasalow, P. Lanzkowsky, *J. Pediatr.* **1992**, *120*, 807.
- [4] L. Osterberg, T. Blaschke, *N. Engl. J. Med.* **2005**, *353*, 487.
- [5] M. T. E. Puts, H. A. Tu, A. Tourangeau, D. Howell, M. Fitch, E. Springall, S. M. H. Alibhai, *Ann. Oncol.* **2014**, *25*, 564.
- [6] M. Viswanathan, C. E. Golin, C. D. Jones, M. Ashok, S. J. Blalock, R. C. M. Wines, E. J. L. Coker-Schwimmer, D. L. Rosen, P. Sista, K. N. Lohr, *Ann. Intern. Med.* **2012**, *157*, 785.
- [7] A. Peterson, L. Takiya, R. Finley, *Am. J. Heal. Pharm.* **2003**, *60*, 657.
- [8] I. Imaz, P. Zegarra, J. Gonzalez-Enriquez, B. Rubio, R. Alcazar, J. Amate, *Osteoporosis Int.* **2010**, *21*, 1943.
- [9] E. Brankin, M. Walker, N. Lynch, T. Aspray, Y. Lis, W. Cowell, *Curr. Med. Res. Opin.* **2006**, *22*, 1249.
- [10] E. Vangeli, S. Bakhshi, A. Baker, A. Fisher, D. Bucknor, U. Mrowietz, A. J. K. Östör, L. Peyrin-Biroulet, A. P. Lacerda, J. Weinman, *Adv. Ther.* **2015**, *32*, 983.
- [11] A. C. Anselmo, S. Mitragotri, *J. Controlled Release* **2014**, *190*, 15.
- [12] E. Porcu, M. Filicori, L. D. Parato, R. Fabbri, R. Seracchioli, C. Colombi, C. Flamigni, *J. Assist. Reprod. Genet.* **1995**, *12*, 15.
- [13] E. Durden, L. Pinto, L. Lopez-Gonzalez, P. Juneau, R. Barron, *Arch. Osteoporosis* **2017**, *12*, 22.
- [14] X. Huang, C. S. Brazel, *J. Controlled Release* **2001**, *73*, 121.
- [15] S. R. Benhabbour, M. Kovarova, C. Jones, D. J. Copeland, R. Shrivastava, M. D. Swanson, C. Sykes, P. T. Ho, M. L. Cottrell, A. Sridharan, S. M. Fix, O. Thayer, J. M. Long, D. J. Hazuda, P. A. Dayton, R. J. Mumper, A. D. M. Kashuba, J. V. Garcia, *Nat. Commun.* **2019**, *10*, 4324.
- [16] L. A. Villarruel Mendoza, N. A. Scilletta, M. G. Bellino, M. F. Desimone, P. N. Catalano, *Front. Bioeng. Biotechnol.* **2020**, *8*, 827.
- [17] A. Kumar, J. Pillai, in *Nanostructures for the Engineering of Cells, Tissues and Organs From Design to Applications*, (Ed.: A. M. Grumezescu), William Andrew, Cambridge **2018**, pp. 473–511.
- [18] H. Zhong, G. Chan, Y. Hu, H. Hu, D. Ouyang, *Pharmaceutics* **2018**, *10*, 263.
- [19] *Strategies to Modify the Drug Release from Pharmaceutical Systems*, (Ed.: M. L. Bruschi), Woodhead Publishing, Waltham, MA. **2015**, pp. 63–86.
- [20] J. T. Santini, M. J. Cima, R. Langer, *Nature* **1999**, *397*, 335.
- [21] A. Servant, L. Methven, R. P. Williams, K. Kostarelos, *Adv. Healthcare Mater.* **2013**, *2*, 806.
- [22] W.-L. Chiang, C.-J. Ke, Z.-X. Liao, S.-Y. Chen, F.-R. Chen, C.-Y. Tsai, Y. Xia, H.-W. Sung, *Small* **2012**, *8*, 3584.
- [23] W. Qin, G. Quan, Y. Sun, M. Chen, P. Yang, D. Feng, T. Wen, X. Hu, X. Pan, C. Wu, *Theranostics* **2020**, *10*, 8179.
- [24] J. Zhang, Y. Zheng, J. Lee, J. Hua, S. Li, A. Panchamukhi, J. Yue, X. Gou, Z. Xia, L. Zhu, X. Wu, *Nat. Commun.* **2021**, *12*, 1670.

- [25] K. T. M. Tran, T. D. Gavitt, N. J. Farrell, E. J. Curry, A. B. Mara, A. Patel, L. Brown, S. Kilpatrick, R. Piotrowska, N. Mishra, S. M. Szczepanek, T. D. Nguyen, *Nat. Biomed. Eng.* **2020**, 23, 998.
- [26] A. C. R. Grayson, I. S. Choi, B. M. Tyler, P. P. Wang, H. Brem, M. J. Cima, R. Langer, *Nat. Mater.* **2003**, 2, 767.
- [27] Y. Xia, D. W. Pack, *Pharm. Res.* **2014**, 31, 3201.
- [28] J. Lee, S. A. Kumar, W. N. Souery, T. Hinsdale, K. C. Maitland, C. J. Bishop, *J. Biomed. Mater. Res., Part A* **2019**, 107, 2160.
- [29] S. Y. Tzeng, K. J. McHugh, A. M. Behrens, S. Rose, J. L. Sugarman, S. Ferber, R. Langer, A. Jaklenec, *Proc. Natl. Acad. Sci. U. S. A.* **2018**, 115, E5269.
- [30] H. Wang, L. Cui, Y. Luo, X. Zhou, R. Liu, Q. Chen, Y. Guan, Y. Zhang, *Biomater. Adv.* **2022**, 137, 212812.
- [31] K. J. McHugh, T. D. Nguyen, A. R. Linehan, D. Yang, A. M. Behrens, S. Rose, Z. L. Tochka, S. Y. Tzeng, J. J. Norman, A. C. Anselmo, X. Xu, S. Tomasic, M. A. Taylor, J. Lu, R. Guaracuco, R. Langer, A. Jaklenec, *Science* **2017**, 357, 1138.
- [32] O. J. A. Schneller, S. T. Brittain, G. M. Whitesides, *Sens. Actuators, A* **1999**, 72, 125.
- [33] S. W. Lee, S. S. Lee, *Microsyst. Technol.* **2007**, 14, 205.
- [34] I. D. Johnston, D. K. McCluskey, C. K. L. Tran, M. C. Tracey, *J. Micromech. Microeng.* **2014**, 24, 035017.
- [35] C. Moraes, Y. Sun, C. A. Simmons, *J. Micromech. Microeng.* **2009**, 19, 065015.
- [36] X. Lu, L. Miao, W. Gao, Z. Chen, K. J. McHugh, Y. Sun, Z. Tochka, S. Tomasic, K. Sadtler, A. Hyacinthe, Y. Huang, T. Graf, Q. Hu, M. Sarmadi, R. Langer, D. G. Anderson, A. Jaklenec, *Sci. Transl. Med.* **2020**, 12, 6606.
- [37] X. Luan, R. Bodmeier, *J. Controlled Release* **2006**, 110, 266.
- [38] H. K. Makadia, S. J. Siegel, *Polymers* **2011**, 3, 1377.
- [39] S. Govardhanagiri, S. Bethi, G. P. Nagaraju, in *Protein Kinase Inhibitors as Sensitizing Agents for Chemotherapy*, (Ed.: B. Bonavida), Elsevier, San Diego, Ca. **2019**, pp. 117–131.
- [40] I. Sadeghi, X. Lu, M. Sarmadi, R. Langer, A. Jaklenec, I. Sadeghi, M. Sarmadi, R. Langer, A. Jaklenec, *Small Methods* **2022**, 6, 2200232.
- [41] K. A. White, B. K. Grillo-Hill, D. L. Barber, *J. Cell Sci.* **2017**, 130, 663.
- [42] R. A. Gatenby, R. J. Gillies, *Nat. Rev. Cancer* **2004**, 4, 891.
- [43] S. Rob Aggarwal, *Nat. Biotechnol.* **2014**, 32, 32.
- [44] L. Urquhart, *Nat. Rev. Drug Discovery* **2021**, 20, 253.
- [45] Y. Chen, T. T. Mutukuri, N. E. Wilson, Q. Tony Zhou, *Adv. Drug Delivery Rev.* **2021**, 172, 211.
- [46] M. Van De Weert, W. E. Hennink, W. Jiskoot, *Pharm. Res.* **2000**, 17, 1159.
- [47] S. Hofmann, C. T. W. P. Foo, F. Rossetti, M. Textor, G. Vunjak-Novakovic, D. L. Kaplan, H. P. Merkle, L. Meinel, *J. Controlled Release* **2006**, 111, 219.
- [48] K. Tsioris, W. K. Raja, E. M. Pritchard, B. Panilaitis, D. L. Kaplan, F. G. Omenetto, *Adv. Funct. Mater.* **2012**, 22, 330.
- [49] J. Garcia, H. I. Hurwitz, A. B. Sandler, D. Miles, R. L. Coleman, R. Deurloo, O. L. Chinot, *Cancer Treat. Rev.* **2020**, 86, 102017.
- [50] R. Varshochian, M. Jeddi-Tehrani, A. R. Mahmoudi, M. R. Khoshayand, F. Atyabi, A. Sabzevari, M. R. Esfahani, R. Dinarvand, *Eur. J. Pharm. Sci.* **2013**, 50, 341.
- [51] S. Y. Tzeng, R. Guaracuco, K. J. McHugh, S. Rose, E. M. Rosenberg, Y. Zeng, R. Langer, A. Jaklenec, *J. Controlled Release* **2016**, 233, 101.
- [52] A. Akinc, M. Thomas, A. M. Klibanov, R. Langer, *J. Gene Med.* **2005**, 7, 657.
- [53] W. Wang, *Protein Sci.* **2015**, 24, 1031.
- [54] M. Duchene, J. Descamps, I. Pierard, in *Medicines from Animal Cell Culture*, (Eds.: G. Stacy, J. Davis), John Wiley & Sons, Ltd, England **2007**, pp. 491–496.
- [55] A. K. Rimpelä, I. Kiiski, F. Deng, H. Kidron, A. Urtti, *Pharmaceutics* **2019**, 11, 9.
- [56] M. Okada, P. Mitchell, R. P. Finger, B. Eldern, S. J. Talks, C. Hirst, L. Paladini, J. Barratt, T. Y. Wong, A. Loewenstein, *Ophthalmology* **2021**, 128, 234.
- [57] M. Ghezzi, S. Pescina, A. Delledonne, I. Ferraboschi, C. Sissa, F. Terenziani, P. D. F. R. Remiro, P. Santi, S. Nicoli, *Pharmaceutics* **2021**, 13, 1476.
- [58] M. Sarmadi, C. Ta, A. M. VanLonkhuyzen, D. C. De Fiesta, M. Kanelli, I. Sadeghi, A. M. Behrens, B. Ingalls, N. Menon, J. L. Daristotle, J. Yu, R. Langer, A. Jaklenec, *Sci. Adv.* **2022**, 8, 5315.
- [59] H. Sun, L. Mei, C. Song, X. Cui, P. Wang, *Biomaterials* **2006**, 27, 1735.
- [60] X. Liu, H. Gu, M. Wang, X. Du, B. Gao, A. Elbaz, L. Sun, J. Liao, P. Xiao, Z. Gu, *Adv. Mater.* **2018**, 30, 1800103.
- [61] R. Varshochian, M. Riazi-Esfahani, M. Jeddi-Tehrani, A. R. Mahmoudi, S. Aghazadeh, M. Mahbod, M. Movassat, F. Atyabi, A. Sabzevari, R. Dinarvand, *J. Biomed. Mater. Res., Part A* **2015**, 103, 3148.